

## Evolution of bioconvective patterns in variable gravity

David A. Noever

Universities Space Research Association, NASA Marshall Space Flight Center, ES-76, Huntsville, Alabama 35812

(Received 25 September 1990)

Measurements are reported of the evolution of bioconvective patterns in shallow, dense cultures of microorganisms subjected to varying gravity. Various statistical properties of this random, quasi-two-dimensional structure have been found: Aboav's law is obeyed, the average vertex angles follow predictions for regular polygons, and the area of a pattern varies linearly with its number of sides. As gravity varies between 1  $g$  and 1.8 $g$  ( $g = 9.8 \text{ m s}^{-2}$ ), these statistical properties continue to hold despite a tripling of the number of polygons and a reduced average polygon dimension by a third. This work compares with experiments on soap foams, Langmuir monolayer foams, metal grains, and simulations.

PACS number(s): 87.45.-k

### I. INTRODUCTION

Cellular patterns appear in a variety of natural problems [1]—soap foams [2,3], Langmuir monolayers [4], metal grains, etc. It has been supposed that unifying principles underly these diverse phenomena. As a consequence, a standard set of statistical tests have been applied to identify universal correspondences. These range from simple cell-side distributions to more formal relations akin to physical laws. An example of the latter is Aboav's law [1]—the product of cell sides,  $n$ , and the average number of neighboring cell sides,  $m$ , is linear in  $n$  ( $mn = 5n + 8$ ). While (in many cases) these relations were originally proposed to describe biological patterns, they have not been applied to a striking biological example of cellular patterns, that arising from bioconvection.

Bioconvection has been known for at least a century and a half [5]. It appears in dense cultures of free-swimming micro-organisms, mostly motile algae and protozoa. Its characteristic feature is the spontaneous self-organization or self-concentration of swimmers into a macroscopic pattern. The pattern arises from a fluid instability, often compared to thermal convection and hence given the name bioconvection [6]. For organisms that are both heavier than their suspending medium (5–10% denser) and that swim upward (due to negative geotaxis, etc.), conditions are set for an unstable density inversion. Heavy organisms accumulate above lighter fluid and a Rayleigh-Taylor instability leads to rapid fluid turnover and self-generating cellular patterns [7,8]. In addition, for many algae, the organisms are bottom heavy (like buoys) and hence have a preferred and stable orientation in coupled gravitational and vorticity fields [9–12]. Where these combined torques sum to zero, downstreams or focal lines appear, and the torques together lead to what has been called gyrotactic swimming. This behavior is important to a large class of motile algae.

For the present purpose, the important feature of these descriptions is their gravity dependence. These theories predict that patterns should disperse in zero gravity. For conciseness, we call these fluid density models.

A second school of thought, however, predicts the opposite outcome, namely that patterns arise not from density differences but directly from the hydrodynamics of swimming, either owing to small vortices generated in the fluid by nearby swimmers [13,14], or due directly to some attractant such as oxygen [15] or electrostatics [16]. These theories are gravity independent and hence predict pattern generation in zero gravity. These are referred to here as wave-reinforcement theories.

We have recently conducted low-gravity tests to differentiate between these competing schools of thought [17]. It was observed that protozoa and algae follow fluid density models, while spermatozoa behavior agrees with wave reinforcement. Herein we report the statistical analysis of cellular patterns driven by fluid density and compare their structure to other pattern-producing phenomena. Results at different gravity levels are contrasted and an extremely simplified fluid model is applied to capture many of the principal observations.

### II. EXPERIMENT

#### A. Organisms and gravity test

Mainly two organisms were used: the motile algae, *Polytomella parva*, and the protozoa, *Tetrahymena pyriformis*. Both were obtained from American Type Culture Collection and grown axenically in recommended aqueous media [18]. These species and their respective bioconvective patterns have been well characterized previously [7,16]. Cultures were incubated at 28°C constant temperature during a 24-h photoperiod (20 lux over 400–700 nm, supplied by cool white fluorescent tubes). Their growth was monitored by cell counting using a hemacytometer.

Within 2–3 d following final seeding, bioconvective patterns were induced by first concentrating the cultures. This was accomplished in 200-ml portions, wherein the cells were harvested by drip filtration [either with 25 psi (absolute) vacuum pressure or without pumping] through a 0.2- $\mu\text{m}$  mesh. Over several hours, the culture volume was allowed to fall to 10 ml, thus yielding a max-

imum organism density of approximately  $10^6 \text{ ml}^{-1}$ .

The patterns were observed in circular plexiglass chambers, 4.8 cm in diameter and between 0.3 and 0.8 cm in depth. The 10-ml lots of concentrated cultures (media plus organisms) were transferred from filters to dishes using 5-ml plastic pipettes. The chambers were completely filled and sealed with fill-port screws such that no free-surface effects or fluid sloshing was possible. It is worth noting that the absence of an air-water interface does not give an obvious source for oxygen gradients; hence the presence of protozoan patterns in our sealed chambers contravenes the previously "definite conclusion that the presence in the medium of a sharp oxygen gradient especially close to the water-air interface is a necessary condition for the appearance of bioconvection in a dense *Tetrahymena* suspension" [15]. Similar findings to ours have been seen by others in sealed chambers before [6] and it is assumed that oxygen appears at a necessary agent only because anoxia leads to slow loss of motility and because motility definitely is necessary for bioconvection.

When photographed against a black background, patterns were visualized by two collimated and remotely cooled incandescent beams angled at  $45^\circ$  and a video camcorder fitted with a macrolens. Although the algae, *P. parva*, is mildly photosensitive, no pattern changes were induced using our exposure time and light intensities.

Variable gravity was induced using NASA's KC-135 research aircraft. It is a modified Boeing 707 Turbojet which by flying a parabolic trajectory alternately obtains 25 s of  $10^{-2}g$  ( $\pm 2 \times 10^{-3}g$ ) during a push-over phase and 20 s of  $1.8\text{--}2g$  during pull-up and pull-out phases. During a typical 2-h flight, it flies 40 parabolas between 7.32 and 10.37 km over the Gulf of Mexico. Following takeoff, cabin temperature remained a constant  $28^\circ\text{C}$ .

### B. Experimental observations

For clarity, experimental presentation will focus on two runs, one each for algae and protozoa, and subsequent statistical analysis will include detailed examination of algal patterns under varying gravity.

Figure 1 shows digitized images of two algal *P. parva* bioconvective patterns at 1 g and 1.8g. The dark regions represent dense lines of falling organisms, whereas the central regions of each polygon include diffusely, upward-swimming organisms. The density difference between dark and light regions is between 25 and 100 times [6]. The number of polygons varies between 20 and 100, with a minimum appearing at higher gravity levels (Table I). The dynamics of these geometric networks does not involve coalescence; rather small (typically three-sided) polygons shrink (called T2 transformation) or vertices exchange (T1 transformation) without changing the number of polygons [1].

The summary of gravitational response is shown in Fig. 2 for two species and two fluid depths. The absence of algal or protozoan patterns in low gravity is consistent

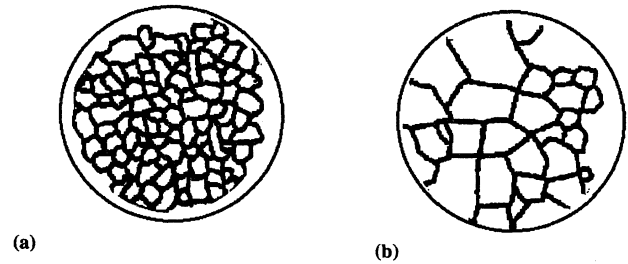


FIG. 1. Digitized images taken of *Polytomella parva* bioconvective patterns at (a) 1 g and (b) 1.8g 30 s later than (a). The shallow samples (0.64 cm) are viewed from above in dishes 3.175 cm in diameter. Flight samples included *Tetrahymena* at a concentration of  $2.2 \times 10^5 \text{ ml}^{-1}$  and *Polytomella* at concentrations of  $1.7 \times 10^6$ ,  $3.2 \times 10^6$ , and  $7 \times 10^6 \text{ ml}^{-1}$ . The digitized images are for a population density of  $3.2 \times 10^6 \text{ ml}^{-1}$ .

with fluid density models and apparently at odds with chemotactic and wave-reinforcement hypotheses.

## III. STATISTICAL ANALYSIS

### A. Number of polygons

A good indicator of organism activity and hence the tendency for pattern formation is the number of polygons [19]. For three cultures, the number of polygons is plotted in Fig. 2 as a function of gravity level. Patterns show a definite cycle that oscillates over six flight parabolas of alternating high, low, and unit gravity. As has been noted in both bioconvection and thermal convection, reducing the chamber depth increases the number of polygons and hence decreases the typical pattern dimension. This will be shown quantitatively in the next section. Shallower cultures show the same cyclical relation to gravity.

A comparison between the two species of bioconvecting organisms shows some variation between polygonal number (roughly half for *Tetrahymena*), but the same oscillation in varying gravity. There has been little work done to compare bioconvection in different organisms, but motility, size, and density change between species and hence give it a characteristic polygonal network.

Since over time there exists a slow loss of motility (owing to anoxia, depletion of carbon energetic sources, etc.), patterns eventually disperse for metabolic, not gravitational, reasons. We have corrected the data of Fig. 2 for this loss of metabolic power by subtracting a least-squared fit to the trend in number of polygons over all gravity levels. This amounts to approximately one polygon lost per minute. The trend-corrected data are shown in Fig. 3 with the middle inset directly comparing the number of polygons for the two species of protists.

The influence of boundaries can be seen for polygons that number less than 100 or so, as was the case in 1.8g patterns (Table I). The role played by boundaries can be made quantitative by scaling the number of wall and bulk patterns with coefficient  $\alpha$ . For soap foams governed by diffusion [2] between patterns,  $N_{\text{wall}}$ , is proportional to

TABLE I. Summary table of organisms tested and gravity dependence of bioconvective patterns in *Polytomella parva*.

Parameter	Species		
	<i>Tetrahymena</i>	<i>Polytomella</i>	<i>Spermatozoa</i>
Dimension ( $\mu\text{m}$ )	30–50	10	2–10
Shape	ellipsoidal	ellipsoidal	ellipsoidal
Typical concentration ( $\text{cm}^{-3}$ )	$10^5$ – $10^6$	$10^6$ – $10^7$	$10^9$
Swimming speed ( $\mu\text{m s}^{-1}$ )	450	100	50–100
Interorganism distance ( $\mu\text{m}$ )	150	50	10
Density ( $\text{g cm}^{-3}$ )	1.076	1.018	1.1
Gravity comparison of patterns			
Average max. dimension (cm)			
1 g		0.48	
1.8g		1.32	
Average no. polygons			
1 g		83	
1.8g		26	
$\alpha$ [boundary effects ( $N_{\text{wall}} = kN_{\text{bulk}}^\alpha$ )]			
1 g		0.84	
1.8g		1.00	

$N_{\text{bulk}}^\alpha$ , where  $\alpha=0.5$  for a large number of polygons. Larger values of  $\alpha$  indicate the influence of walls. Particularly for the high-gravity patterns, boundary effects ( $\alpha=1$ ) appear and distort the distribution of polygonal sides,  $n$ ; this will be shown in Sec. II C.

As shown in Fig. 4, the logarithm of the average number of polygons shows a peak at unit gravity. This peak should not be interpreted too rigorously, as it represents an interpolation between three gravity levels only. In fact, a more convincing argument is that the zero-gravity

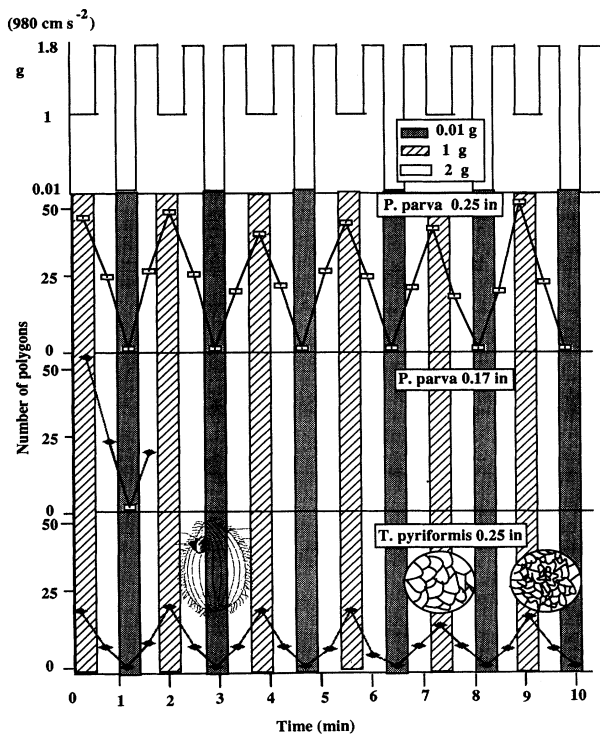


FIG. 2. The number of polygons as a function of gravity. The top graph depicts the step function ( $\pm 0.002g$ ) in gravity achieved by parabolic flights. The lower graphs depict the number of polygons at varying gravity levels for the two species as marked. The inset at lower right shows a schematic of the digitized patterns; the inset at lower left shows the 50- $\mu\text{m}$  protist, *Tetrahymena*.

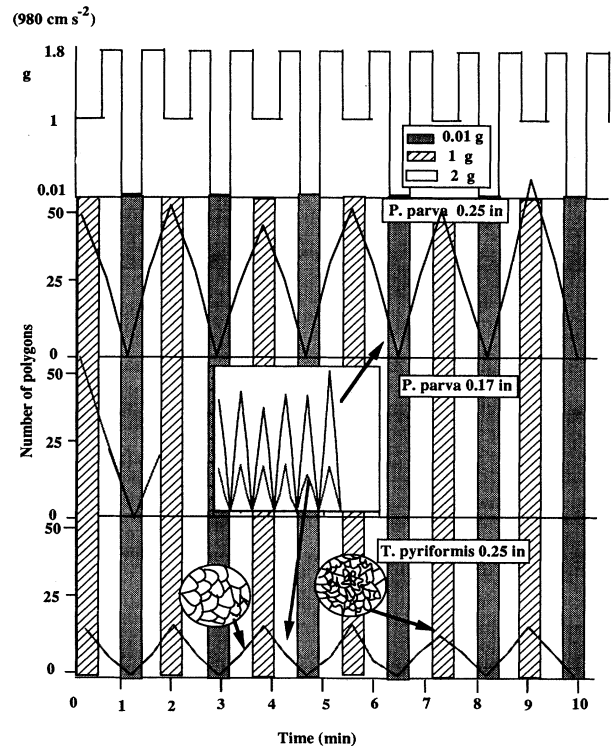


FIG. 3. Trend-corrected data for Fig. 2. A least-squares fit of the number of polygons has been subtracted from 1 g and 1.8g results to account for the slow loss of motility over several parabolas. This effect presumably arises from anoxia, depletion of carbon sources, etc. The middle inset directly compares the number of polygons for the two species, with the upper jagged line applying to *P. parva*.

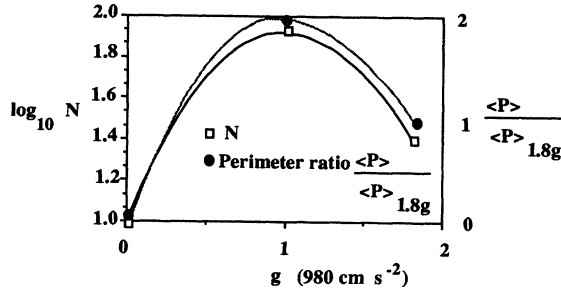


FIG. 4. A semilog plot of average number of polygons for *P. parva* as a function of gravity and of the perimeter ratio (scaled to the case for 1.8g). Each point is the average of eight parabolas.

limit corresponds not to  $N=0$ , but rather to  $N=\infty$ . This view not only removes the arbitrary uniqueness of unit gravity, but also has strong analogies to the zero-thickness limit in Benard-Marangoni convection.

An interesting comparison between the log number of polygons and the ratio between the computed perimeter ratios for polygonal networks shows remarkably similar behavior as gravity is varied. This can be demonstrated explicitly by a linear plot of perimeter ratio as a function of the log number of polygons (Fig. 5). Such a relation has apparently not been advanced previously for other polygonal networks. It would be interesting to test this kind of relation experimentally in, for example, Langmuir monolayers using component concentrations rather than gravity as the relevant variable.

### B. Area

Table I summarizes the direct comparison between the same pattern-forming culture (*P. parva*) separated by 20 s in two gravity fields. If, following Berge [20], we compute the average polygonal area by dividing the available surface area by the total number of polygons for repeated

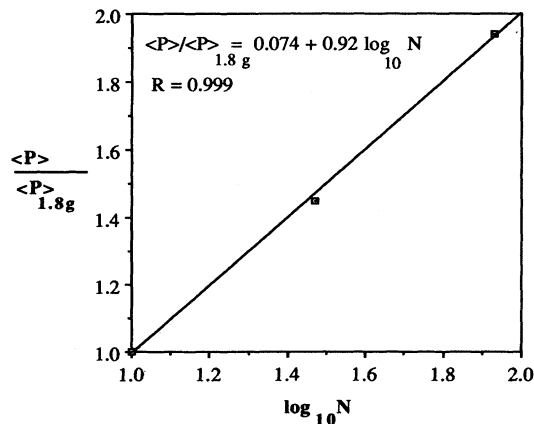


FIG. 5. A least-squares fit of the perimeter ratio (Fig. 4) plotted against the log of the number of polygons. Parameters of the fit are shown for the inset. Each data point is the average of eight parabolas.

runs, the average area from seven parabolic flights is shown for both algae and protozoa in Fig. 6. The rise in pattern area can similarly be interpreted as an increase in the characteristic maximum dimension,  $D=(4A)^{1/2}/\pi$ . This is shown in Fig. 7.

### C. Polygon-side distributions

Since theory [1] has described the coarsening of networks using area and side distributions, these are the primary experimental parameters of statistical interest. For an infinite space-filling two-dimensional network with trigonal vertices, the Euler relation gives  $\langle n \rangle = 6$  for the average number of sides in a polygon (first moment). Since bioconvection polygons are quasi-two-dimensional, the first moment differs from six, as shown in Fig. 8. However, the first moment remains constant for the two gravity levels tested, indicating that boundary effects do not appear to change selection of polygonal sidedness.

An empirical relation governing the number of polygonal sides and  $m$ , the average number of sides for neighboring polygons, is attributed to Aboav [1]:

$$mn = 5n + 8. \quad (1)$$

This is plotted as the uppermost dark solid line in Fig. 9. Bioconvective networks deviate from this correlation with a least-squares fit agreeing better with the Aboav-Weaire relation [1] found valid for soap foams,

$$mn = (6-a)n + (6a + \mu_2), \quad (2)$$

where  $a$  is a constant of order unity and  $\mu_2$  is the second moment of the polygon-side distribution,  $p(n)$ :

$$\mu_2 = \sum_n p(n)(\langle n \rangle - n)^2. \quad (3)$$

Values of  $a=0.75$  and  $\mu_2=0.55$  were found to match independently with the least-squares fit of  $mn$  vs  $n$  and a direct calculation using (3) for  $\mu_2$ . Within the limits of our analysis, this agreement is reasonable. The second moment does vary with gravity as shown in Fig. 9, indicating that, unlike the first moment, the second moment

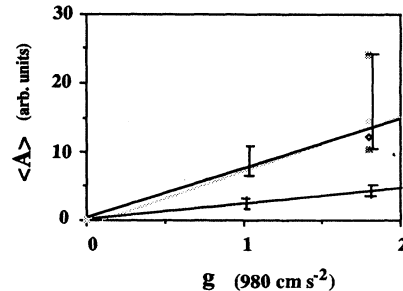


FIG. 6. Average polygonal area as a function of gravity level. The top line holds for *Tetrahymena* and the bottom line for *Polytomella*. Vertical lines represent the spread between different parabolas. A least-squares fit to *Polytomella* data has a correlation coefficient  $R=0.974$  for  $\langle A \rangle = 1.5g - 0.02$ . A least-squares fit to *Tetrahymena* data has a correlation coefficient  $R=0.999$  for  $\langle A \rangle = 7.9g - 0.85$ .

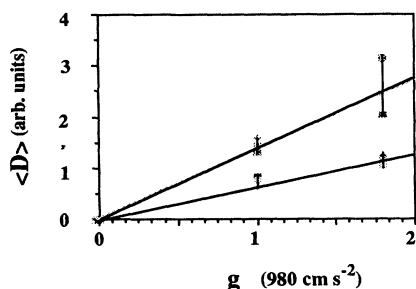


FIG. 7. Average maximum polygonal dimension ( $D=2A^{1/2}/\pi$ ) as a function of gravity level. The top line holds for *Tetrahymena* and the bottom line for *Polytomella*. Vertical lines represent the spread between different parabolas. A least-squares fit to *Polytomella* data has a correlation coefficient  $R=0.978$  for  $\langle D \rangle=0.6g-0.06$ . A least-squares fit to *Tetrahymena* data has a correlation coefficient  $R=0.999$  for  $\langle A \rangle=1.4g-0.03$ .

does reveal a change in network morphology for higher-gravity levels. For example, higher-gravity patterns show a peak number of five-sided polygons, where unit gravity peaks at six sides. Further analysis of this variation for boundary effects and equilibrium patterns is a challenging problem, because in contrast to diffusion-dominated effects in soap foams, bioconvection includes diffusion, bulk convection, and swimming, each of which competes to give polygonal networks.

Plotted as a function of gravity, the complete distribution functions for polygon sides are shown in Fig. 10. As mentioned previously, gravity plays a role in selecting the maximum in the side distribution at five for higher gravity and six for unit gravity. Given, however, that the average remains the same and that the variation between runs is likely to be significant, this variation appears to be in line with what has been observed for soap foams be-

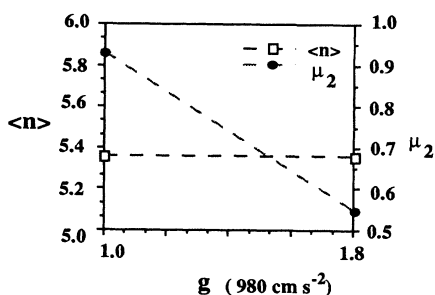


FIG. 8. First  $\langle n \rangle$  and second moments ( $\mu_2$ ) of the polygonal side distributions  $p(n)$  for *Polytomella* as a function of gravity. For the two gravity levels averaged over eight parabolas, the average sidedness is approximately 5.4 independent of gravity and the second moment varies inversely with gravity. The dashed lines are schematic only; no intermediate gravity levels were experimentally accessible and linear behavior is not implied. The trends are indicated for comparison. The second moment in terms of the probability  $p(n)$  of an  $n$ -sided pattern is found within a general network  $\sum_n p(n)(\langle n \rangle - n)^2$  with average  $\langle n \rangle$ .

tween five and six sides and nearly equal probabilities for comparison runs. This topic will be examined again in the discussion when bioconvective results are compared to simulations and related experiments.

#### D. Vertex angles

Stability arguments require that a two-dimensional foam should converge to a vertex angle of  $120^\circ$ . This has been shown from experiment [20] for foam structures in Langmuir monolayers  $\pm 13^\circ$ . We have measured the distribution of angles as a function of  $n$  for gravity between 1 and 1.8g. For digitized images of the network, the angles were measured with a protractor for different numbers of sides; the result is shown in Fig. 11. The weighted average

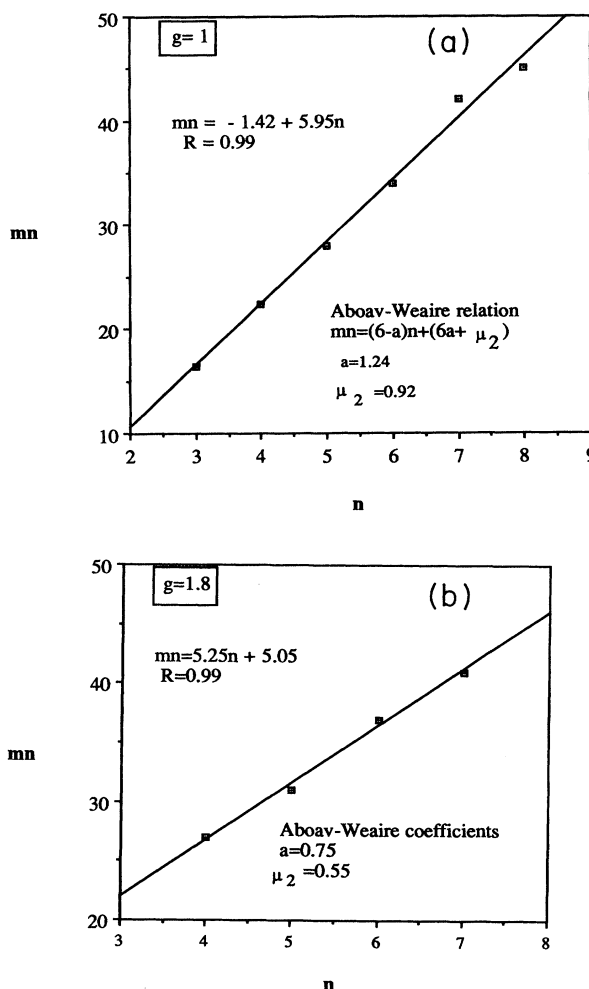


FIG. 9. Test of Aboav-Weaire's law for bioconvective polygons of *Polytomella* patterns as a function of gravity. All gravity levels indicate a correlation between the number of sides of a polygon,  $n$ , and the average number of sides of its neighbors,  $m(n)$ . (a) For  $g=1$ . (b) Least-squares fit (LSF) of the data for  $g=1.8$ . Parameters fitting Weaire's relation (see text) give  $a=0.75$ ,  $\mu_2=0.55$ .

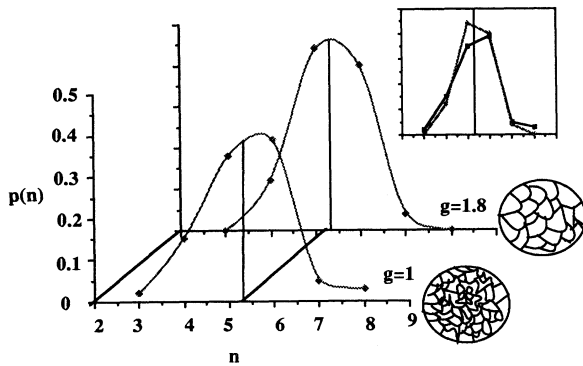


FIG. 10. *Polytomella* bioconvective pattern cell-side distribution for varying gravity. Insets above the  $x$  axis show digitized pictures of actual pattern changes, with  $p(n)$  expressing the fraction of  $n$ -sided cells. Inset at upper right shows an overlay of the two distributions for direct comparison, with the high-gravity result having a peak at polygon sides of five, and the unit gravity result having a peak at polygon sides of six.

$$\langle \Phi \rangle = \sum_n \Phi(n)p(n)$$

is summed over all angles with  $n$  sides, giving the average for each  $n$  of  $\Phi(n)$ . This average is then weighted by the probability  $p(n)$  of finding an  $n$ -sided polygon; the result is  $111^\circ \pm 11^\circ$ , with a broad distribution of angles for each  $n$ . Also plotted in Fig. 11 is the expected vertex angle for regular polygons, which, as one might expect, follows the trend appearing in the data. Within the variation between separate runs, the gravity dependence of vertex angles is not significant.

#### E. Area distribution for different sidedness

From studies of biological systems, Lewis concluded that the average area of a polygon  $\langle A_n \rangle$  should vary linearly with the number of sides. This has been called Lewis's law [21], although it has never been used to analyze bioconvective patterns. It is known to hold for mathematical mosaics generated by Voronoi construction [1], but for soap foams and grain boundaries, area plots

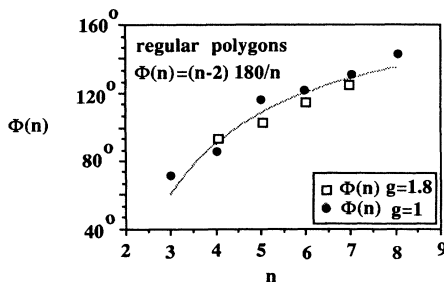


FIG. 11. *Polytomella* bioconvective pattern average vertex angles as a function of the number of sides for different gravity levels. The plotted line is the geometrically expected angle for regular polygons of  $n$  sides with the governing equation (inset, upper left).

do not agree as well as an equivalent linear plot of perimeter as a function of sides. As shown in Fig. 12, bioconvective results are ambiguous in this regard. The average area was computed from pixel counts of digitized polygons and varies linearly (correlation coefficient,  $R=0.96$ ) for unit gravity, in accord with Lewis's law. In contrast, however, agreement with this relation seems to have a gravity dependence, such that high gravity decreases the area occupied by polygons with fewer than six sides. One reason for this difference may be boundary effects arising from the fewer number of high-gravity polygons; boundaries may, for example, stabilize normally shrinking (T2) polygons with a small number of sides. This speculation is supported by the marked contrast between area distribution functions (Fig. 13) wherein the broader high-gravity distribution shows a higher probability for finding small polygons with five or fewer sides.

#### IV. AN ANALYTICAL MODEL

Bioconvection has generated much theoretical work recently [8–12, 22–25]. However, a universal model capable of uniting many different kinds of bioconvection has

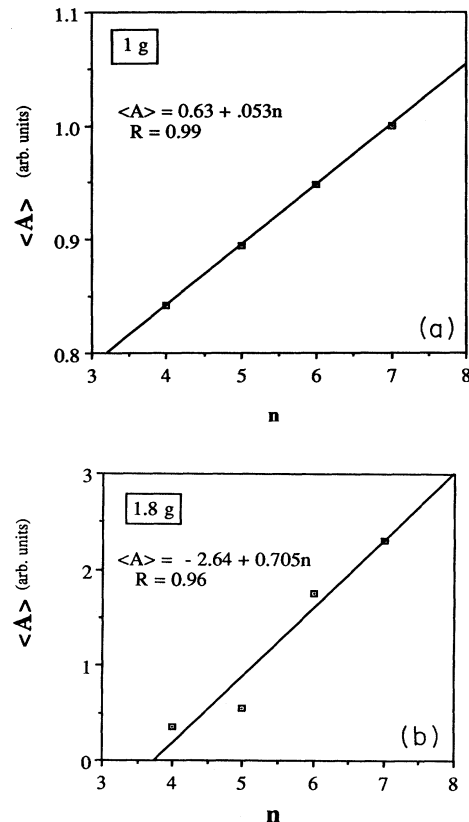


FIG. 12. Average polygonal area  $\langle A_n \rangle$  as a function of  $n$  sides for bioconvective polygons of *Polytomella* patterns for different gravity levels, (a)  $g=1$  and (b)  $g=1.8$ . Data for unit gravity indicate a linear fit would be appropriate, in accordance with Lewis's law. Least-square-fit parameters are shown at upper left for unit gravity.

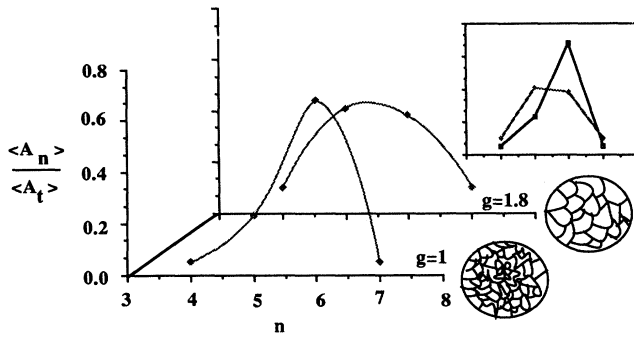


FIG. 13. Probability distribution for area as a function of  $n$  sides for bioconvective polygons of *Polytomella* patterns for various gravity levels. Insets above the  $x$  axis show digitized pictures of actual pattern changes, with  $p(A)$  expressing the fraction of area occupied by  $n$ -sided cells. Inset at upper right shows an overlay of the two distributions for direct comparison, with the unit gravity result having a peak at polygon sides of six, and the high-gravity result having a peak at polygon sides of five.

not been proposed and may not prove realizable for the wide variety of organisms known to form dynamic patterns (e.g., flagellates, ciliates, sperm, zoospores, large bacteria, and certain invertebrates). In particular, the protists we tested (the ciliate *Tetrahymena*, and the flagellate *Polytomella*) do not conform uniformly to previous theories. As an example, the flagellate has been observed to form density-stable fingers flowing upward into less-dense media [26]—an experimental observation that contrasts markedly with expectations of a simple Rayleigh-Taylor instability (heavy over light fluid). Likewise, although *Tetrahymena* has all the characteristics of a gyro-tactic swimmer [27] (e.g., a rotary swimming trajectory with its gravity center displaced downward from its drag center), it apparently does not bioconvect using this mechanism [28]. The reason for this is unknown. In part, this variability (both between species and between theory and experiment) motivated the present test for gravitational responses of macroscopic patterns. These varied conditions for bioconvection also suggested that it might prove of interest to set up a simple pattern analytically and to see what kinds of bioconvecting paths or trajectories can be described successfully.

#### A. The Stommel model

Each closed pattern is modeled as rotating about a central axis. The rotational sense of a given pattern is opposite to its immediate neighbors, much like the rotation of a long train of gears. Such gear motion has been observed experimentally for the motile algae, *Euglena viridis* [5], and *Tetrahymena* [7] and predicted from various general analytical models [29]. Figure 14 shows a vertical cross section of two such neighboring closed circuits. Nothing will be said about the onset of this initial flow. The curved trajectories are streamlines of constant velocity and the problem is treated as two dimensional.

At the low Reynolds numbers typical of small-scale

swimming, the organisms move with the fluid streamlines. Their motion, if scaled to human size, would amount to a slow crawl through molasses [30]. Since the organisms become entrained with the fluid once fully developed convection sets in, an added feature of a streamline model is its relative freedom from the particulars of propulsion. This proves of interest since similar bioconvective patterns arise in dissimilar swimmers—flagellates, ciliates, ameboids, and even motile colonies (e.g., *Volvox*), as well as gyrotactic and nongyrotactic swimmers.

Since all modeled micro-organisms have densities larger than their suspending fluid, Stokesian dynamics will describe their aggregative activity [31]. To trace any trajectory other than vertical downward motion along a straight line, the modeled micro-organisms must show negative geotaxis (swim against gravity). Further, only those micro-organisms that swim upward faster than their settling velocity can form closed paths. These closed circuits provide the basis for a simple bioconvective model (sometimes called the Stommel model [32] elsewhere in the analysis of wind-driven surface flows), wherein observed patterns are considered as regions of active trapping.

The coordinates of a micro-organism are  $(x, y)$ , both of which are functions of time  $t$ . The horizontal velocity of a micro-organism is  $dx/dt$ , while the vertical velocity is  $dy/dt$ . The fluid motion may be specified by a stream function that, in general, is arbitrary. The horizontal and vertical fluid velocities are

$$\mathbf{v} = \left[ \frac{\partial \psi}{\partial y}, -\frac{\partial \psi}{\partial x} \right]. \quad (4)$$

If the organism settling velocity is  $V$ , then

$$\frac{dx}{dt} = \frac{\partial \psi}{\partial y}, \quad \frac{dy}{dt} = -\frac{\partial \psi}{\partial x} - V. \quad (5)$$

Using a trial function  $\psi_1$ , these equations can be transformed:

$$\frac{dx}{dt} = \frac{\partial \psi_1}{\partial y}, \quad \frac{dy}{dt} = -\frac{\partial \psi_1}{\partial x}. \quad (6)$$

The trial function  $\psi_1$  is therefore given by

$$\psi_1 = \psi + Vx, \quad (7)$$

where the trajectory of a micro-organism is a curve along which  $\psi_1$  is constant. In the case of bioconvection patterns, the simplest stream function to consider is

$$\psi = \psi_0 \sin x \sin y. \quad (8)$$

This stream function gives two neighboring patterns with a roll-like structure. In this case, the trajectories are given by

$$\frac{\psi_1}{\psi_0} = \sin x \sin y + \beta x, \quad (9)$$

where, with dimensions of inverse length, the quantity  $\beta$  is defined by

$$\mathfrak{R} = \frac{V}{\psi_0} \tag{10}$$

The trajectories for resultant organism velocities can be written as a function of a dimensionless quantity  $\mathfrak{R}$ , the

ratio of the settling velocity to the maximum upward swimming velocity.

Pattern variation with fluid and micro-organism properties are shown in Fig. 14. If  $\mathfrak{R}$  is large ( $\mathfrak{R} > 1$ ), the trajectories are essentially straight vertical lines and settling

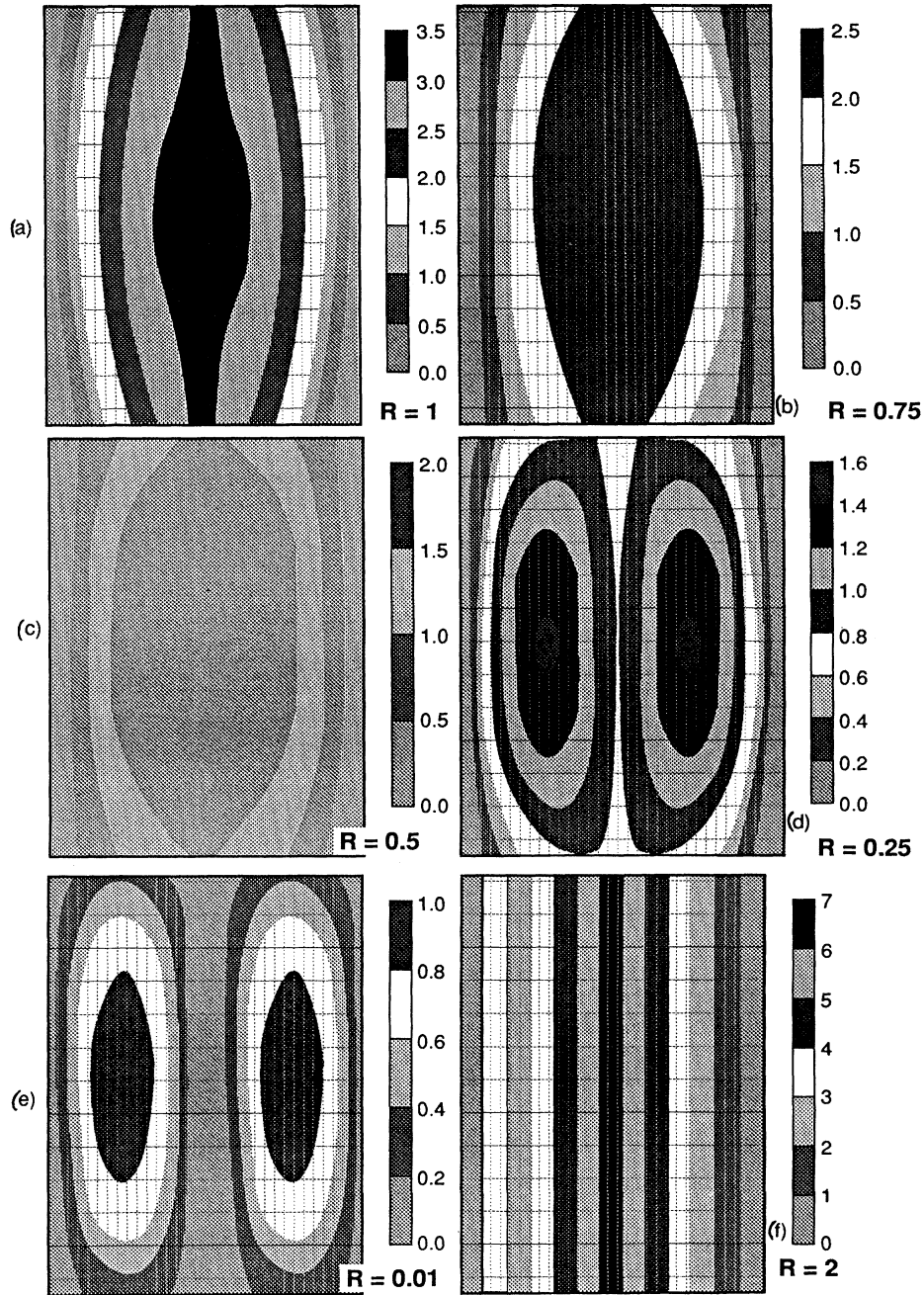


FIG. 14. Variation of micro-organism trajectories with motility as predicted by analytical model. Differently shaded regions indicate boundaries for different streamlines of constant velocity.  $\mathfrak{R}$  is the dimensionless settling velocity (normalized to the swimming velocity). Velocity scales are shown at right of each streamline map. 1(a) shows the onset of closed trajectories and pattern formation; 1(b)–1(e) show intermediate values, wherein successively higher swim velocities and sample motility yield more intricate pattern formation; 1(f) shows the dead limit of no pattern formation and complete sedimentation.  $\mathfrak{R} = (Ga/Re)(1 - \rho_{org}/\rho_{soln})$ ; the density ratio,  $(\rho_{org}/\rho_{soln}) > 1$ ; Galileo number,  $Ga = gr^3/v^2$ ; Reynolds number,  $Re = vr/v$ .

dominates upward swimming. As  $\mathcal{R}$  approaches unity the trajectories begin to bow outward such that, although all micro-organisms eventually settle, those nearest the central region of maximum upward velocity fall more slowly.

If  $\mathcal{R}$  is less than unity ( $0 < \mathcal{R} < 1$ ), there are regions of active trapping where the micro-organisms swim upward at a sufficient rate to counteract settling. The interesting feature of this case is that there exist closed trajectories that model bioconvective patterning. The trajectories farthest from the central region are not closed, since upward velocity is a minimum and settling dominates. Clearly the trapping region (closed circuits) becomes larger as  $\mathcal{R}$  approaches zero (i.e., higher motility). This parallels the density magnification (or dimpling) observed in bioconvective pattern formation.

Since pattern formation depends on the ratio between settling and swimming speeds, this analysis yields the following simple relation:

$$\frac{v}{v_{\text{swim}}} = \frac{2}{9} \frac{gr^2}{v_{\text{swim}} v} \left[ \frac{\rho_{\text{org}}}{\rho_{\text{soln}}} - 1 \right] = \frac{2}{9} \frac{\text{Ga}}{\text{Re}} \left[ \frac{\rho_{\text{org}}}{\rho_{\text{soln}}} - 1 \right], \quad (11)$$

where the dimensionless Galileo number  $\text{Ga} = gr^3/v^2$  indicates the relative importance of gravity to viscous effects, the Reynolds number  $\text{Re} = v_{\text{swim}} r/v$  indicates the relative importance of swimming velocity to viscous effects ( $\text{Re} < 1$ , for micro-organism swimming), and the density ratio will be assumed greater than unity. The parameter  $r$ , the organism radii, can be treated here as a fitted parameter that includes the collective effects of settling.

Critical patterns for pattern formation follow for  $\mathcal{R} = v/v_{\text{swim}} = 1$ , whereupon the model would first show bioconvective patterns,

$$\left[ \frac{\rho_{\text{org}}}{\rho_{\text{soln}}} - 1 \right] \frac{\text{Ga}_c}{\text{Re}_c} \leq 4.5. \quad (12)$$

Particularly when many variables such as density, radius, and swimming speed vary simultaneously from organism to organism, or when solution media have different viscosities and densities, this dimensional approach proves advantageous. The darkened wedge shown in Fig. 15 indicates the available region for bioconvective pattern formation as a function of solution and micro-organism properties.

### B. Formation rate for bioconvection patterns

For bioconvective patterns, it is of interest to get a measure of the maximum formation rate as a function of swimming speed. As two examples to test the validity of the Stommel model, the present results predict the viscosity dependence of the formation rate and the temperature dependence of faceting in equilibrium patterns.

For  $\mathcal{R} = v/v_{\text{swim}} < 1$ , the minimum formation time is assumed to equal the time required to complete one circulation of a square bioconvective cell with characteristic dimension  $L$ . The time required to swim up a length  $L$  is

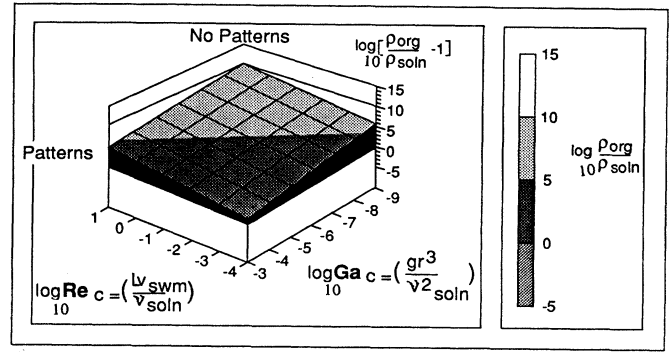


FIG. 15. Minimum density ratio ( $\rho_{\text{org}}/\rho_{\text{soln}}$ ) of organisms required for pattern formation. Values shown as a function of critical Reynolds and Galileo numbers for  $10^{-3} < \text{Re} < 10$  and  $10^{-8} < \text{Ga} < 10^{-3}$ . The darkened wedge indicates the densities that yield patterns.

$$t_{\text{up}} = \frac{L}{v_{\text{swim}} - v} = \frac{L}{v \left[ \frac{1}{\mathcal{R}} - 1 \right]}, \quad (13)$$

the time required to swim across  $2L$  is

$$t_{\text{across}} = \frac{2L}{v_{\text{swim}}} = \frac{2L\mathcal{R}}{v}, \quad (14)$$

and the time required to swim down a length  $L$  is

$$t_{\text{down}} = \frac{L}{v}. \quad (15)$$

[In writing the time required to swim down, bunching of micro-organisms is assumed to lead to settling only without competing upward swimming; this accounts for the asymmetry between (13) and (15). This has been observed repeatedly (see, e.g., Ref. [5]). Without this assumption, unphysical negative swim times would be possible for  $\mathcal{R} < 1$ .]

Summing the total times gives

$$t_{\text{formation}} = \frac{L}{v} \frac{2\mathcal{R} - 1}{\mathcal{R} - 1}, \quad (16)$$

and a maximum possible formation rate, in  $s^{-1}$ ,

$$\xi = \frac{\mathcal{R} - 1}{2\mathcal{R} - 1} \frac{2gr^2(\rho_{\text{org}}/\rho_{\text{soln}} - 1)}{9Lv} = \frac{\mathcal{R} - 1}{2\mathcal{R} - 1} \Omega. \quad (17)$$

Here  $\Omega$  is defined as the characteristic pattern frequency for nonswimming micro-organisms (dead limit).

In both the limit of no settling (as  $\mathcal{R}$  goes to zero) and total settling (as  $\mathcal{R}$  goes to unity), this formation rate goes to zero and thus appropriately predicts no bioconvective patterns. Written as a function of characteristic pattern frequency, the intermediate  $\mathcal{R}$  values ( $0 < \mathcal{R} < 1$ ) give pattern formation rates shown in Fig. 16. As has been observed [6], more motile micro-organisms show both faster formation rates and smaller characteristic pattern dimensions  $L$ . A qualitative comparison of our flight results in varying gravity and pattern variation predicted by the present simple model using closed trajectories is shown in Fig. 17.

### C. Viscosity dependence of pattern formation

These model predictions agree quantitatively with the experiments of previous workers. Available work [33] on the variation of pattern-formation rate with viscosity is plotted in Fig. 18. For small additions (2, 4, and 6 wt. %) of methyl cellulose, the kinematic viscosity was varied by a factor of 4 ( $0.01 < \nu < 0.04 \text{ cm}^2 \text{ s}^{-1}$ ), with a consequent increase in pattern-formation time. Equation (14) predicts that the formation rate (in  $\text{s}^{-1}$ ) varies inversely with the first power of viscosity,

$$\xi = \frac{K}{\eta}, \quad (18)$$

where  $\eta$  (in  $10^{-2} \text{ g/cm s}$ ) is the viscosity of suspending solution, and for a given micro-organism,  $K$  is a constant. For small additions of methyl cellulose, this analysis neglects the change (typically less than 2%) in solution density.

As shown in Fig. 18, there is agreement between re-

ported values and the model predictions (with  $K = 1.6 \times 10^{-3} \text{ g cm}^{-1} \text{ s}^{-2}$  for *Tetrahymena*). At the lower viscosities in Fig. 18, the model predicts a faster formation time compared to experiment [33]. Here, the faster swimming rates (expected at lower viscosities) are likely to lead to collective effects unaccounted for in this simple model based on free circulation rates.

In a qualitative sense, one can similarly connect the degree of pattern faceting with viscosity. As viscosity increases, values of  $\mathcal{R}$  decrease such that, as shown in Fig. 14, patterns would be expected to become finer. This observation is discussed in more detail in the following section.

### D. Thermal dependence of viscous pattern formation

Thermal changes have two consequences for pattern formation. First, a decrease in temperature slows formation rates, and second, a decrease in temperature results in finer patterns with increasing faceting. One can imag-

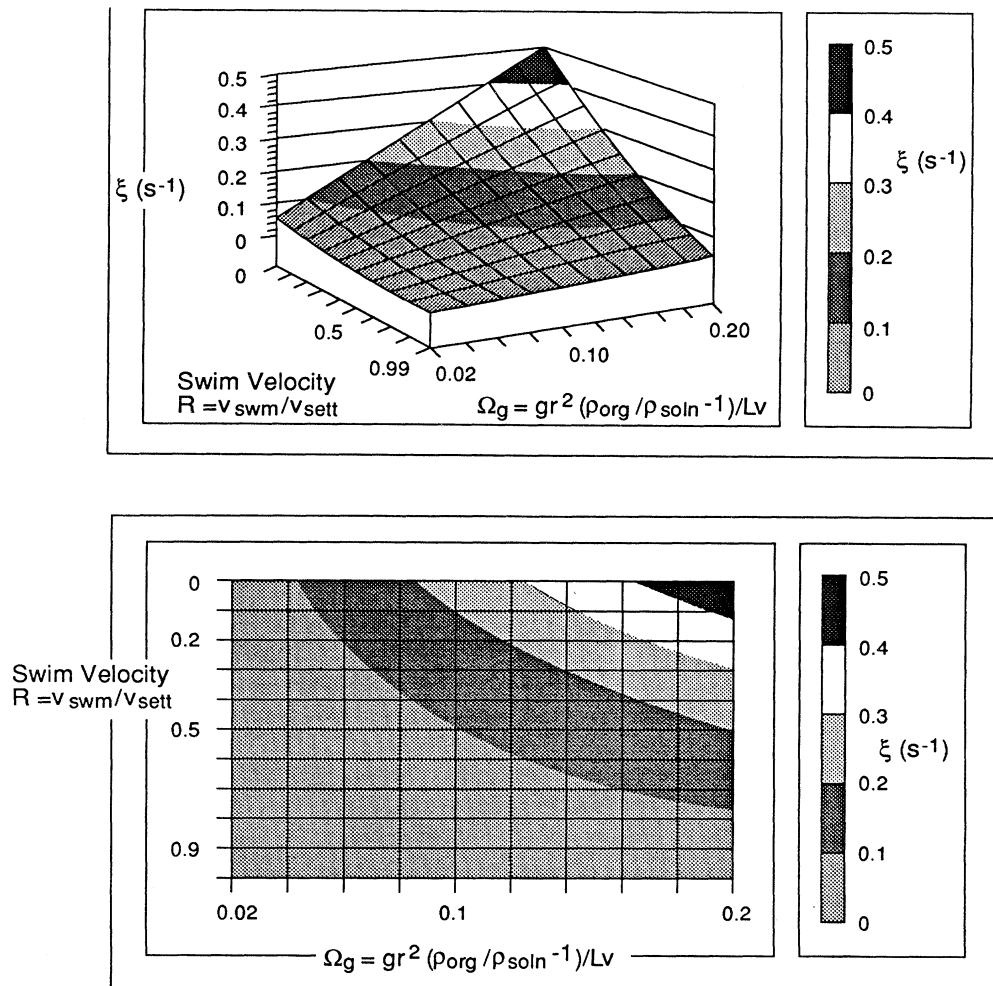


FIG. 16. Variation of bioconvective pattern-formation rate as a function of solution and micro-organism properties. The upper and lower panels show surface and contour maps, respectively, of the variation of formation rate with swimming velocity and pattern size.

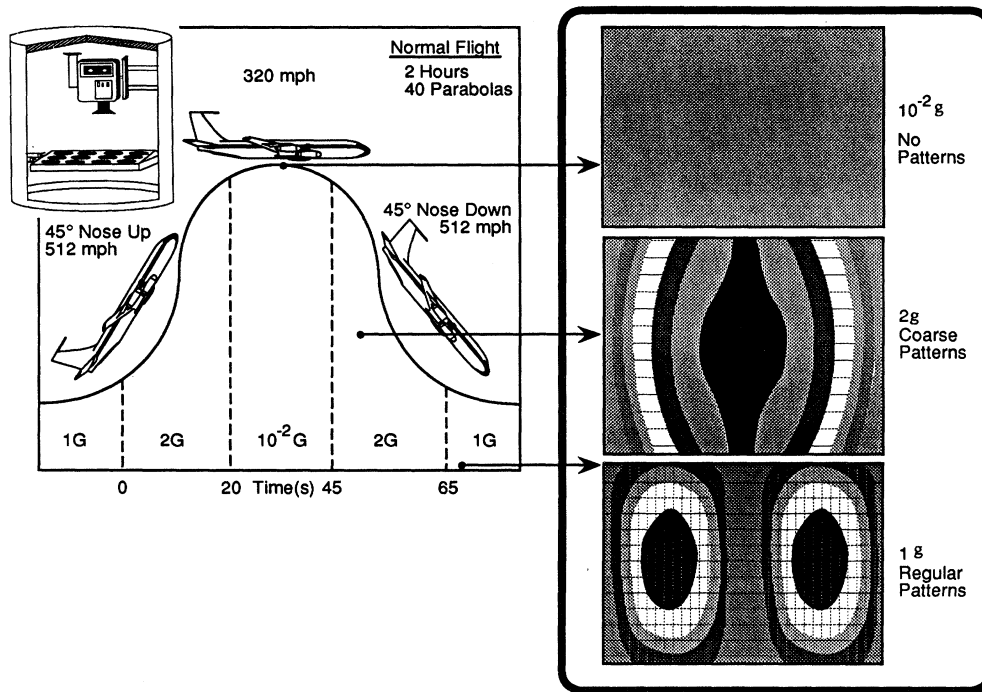


FIG. 17. Qualitative comparison of flight results with the Stommel-model predictions. The experimental cannister is shown schematically at upper left (camcorder plus shallow dishes for cultures); the flight trajectory is shown in the middle and the model results for protist patterns are shown at right at various gravity levels.

ine that pattern formation will show a complex thermal dependence, relying on metabolic activity, solution viscosity, and density changes. In the spirit of the previous example, the present model can most easily deal with viscosity as a thermal parameter. The more interesting connection between micro-organism properties and their relation to both temperature and pattern formation will await future work.

A generally satisfactory model for estimating viscosities in liquids is scarce. Following a suggestion by Rey-

nolds [34], viscosity is often presented via an Arrhenius relation

$$\eta = A \exp(E_\eta / RT), \quad (19)$$

where  $A$ ,  $R$  (gas constant), and  $E_\eta$  (a viscous activation energy) are temperature insensitive. For water between  $0^\circ\text{C}$  and  $40^\circ\text{C}$  at 1 atm pressure, a linear fit of  $\ln \eta \cdot \cdot 1/T$  correlates with correlation coefficient  $R^2=0.999$  [see Fig. 19(a) for plotted data]. Hence by including viscosity changes alone, one would expect pattern-formation rates to decrease with decreasing temperature,

$$\xi = K / [A \exp(E_\eta / RT)], \quad (20)$$

or, taking the fitted parameter  $K$  from Fig. 18 for *Tetrahymena* ( $K=1.6 \times 10^{-3} \text{ g cm}^{-1} \text{ s}^{-2}$ ) in water ( $A=0.7 \times 10^{-5} \text{ P}$ ,  $E_\eta/R=2.1 \times 10^3$ ),

$$\xi = (2.29 \times 10^2) / \exp(2100/T), \quad (21)$$

with  $\xi$  in  $\text{s}^{-1}$  and  $T$  in K. Figure 19(b) shows predicted formation times as a function of temperature. Although Loeffler and Mefferd [33] reported only a single datum of temperature-formation time for *Tetrahymena*, the model prediction for pattern formation at  $20^\circ\text{C}$  is the correct order. Across the temperature interval between  $0^\circ\text{C}$  and  $40^\circ\text{C}$ , formation rates (inverse time) approximate a direct proportionality to temperature, as was also reported experimentally. Hence, given a particular temperature, this model can predict pattern-formation rates using viscosity

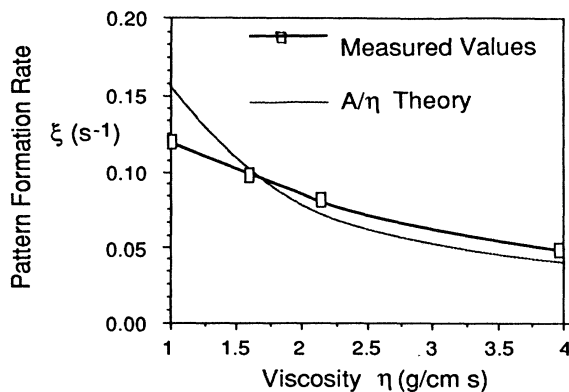


FIG. 18. The correspondence between the analytical model and Loeffler and Mefferd (Ref. [33]) data, open rectangles, for viscosity dependence of the pattern-formation rate.

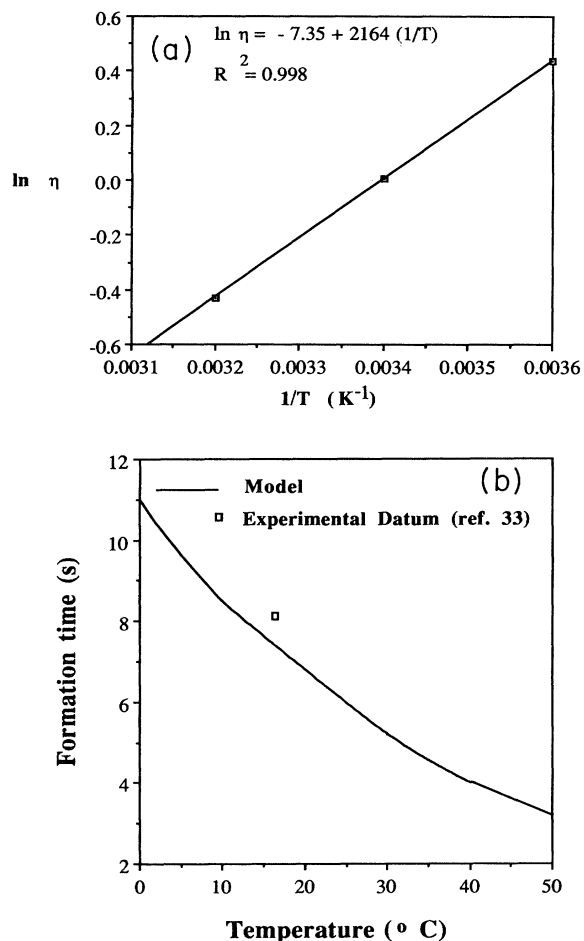


FIG. 19. (a) Temperature dependence of viscosity for water between 0 and 40 °C. (b) Predicted temperature dependence of formation times. The solid line indicates predicted values from the analytical model and the Loeffler and Mefferd (Ref. [33]) datum for temperature.

as the varying parameter.

Similarly, Fig. 14 can be used to predict the change in fine structure due to cooling a culture. The value of the dimensionless velocity  $\mathcal{R}$  varies inversely with kinematic viscosity  $\nu$ :

$$\mathcal{R} \propto \nu^{-1}, \quad (22)$$

such that for decreasing temperature (and consequently, increasing viscosity),  $\mathcal{R}$  will decrease and patterns will follow the change in aspect from Figs. 14(a) to 14(e). This connects well with the qualitative observations [33] of “patterns becoming progressively finer and containing smaller facets.”

## V. CONCLUSIONS

Experiments are reported that analyze statistically the response of bioconvective patterns to variable gravity. An oxygen attractant can be ruled out as a necessary

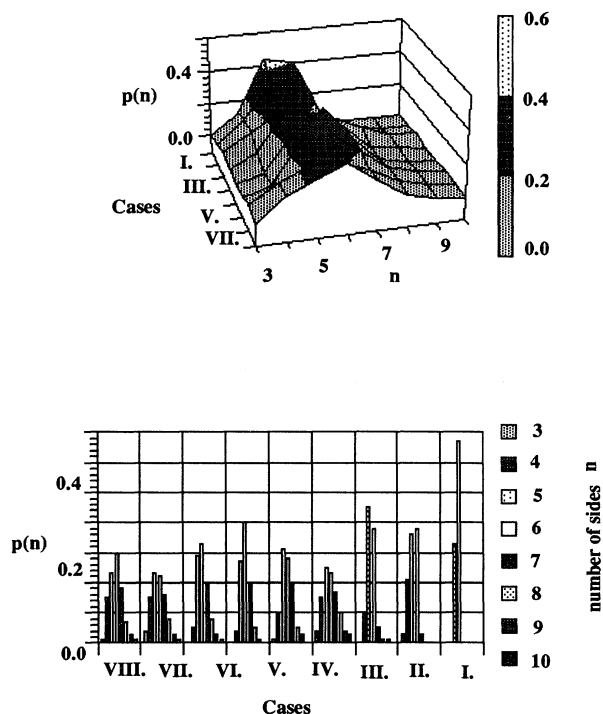


FIG. 20. Comparison of polygon-side distributions from the present bioconvective experiment, from various work on foams, and numerical simulations. Some universal characteristics appear as seen in the following: cases I and II, this bioconvective work on gravity levels; case III, the Potts model, Srolovitz *et al.* (Ref. [35]); case IV, soap foams, Stavans and Glazier (Ref. [3]); case V, continuum model, Beenakker (Ref. [36]); case VI, vertex model I, Kawasaki, Nagai, and Nakashima (Ref. [37]); case VII, vertex model II, Kawasaki, Nagai, and Nakashima (Ref. [37]); case VIII, Langmuir monolayers of foam (Ref. [20]).

agent for bioconvection. Polygonal networks are shown to follow Aboav’s law and Lewis’s law governing polygonal sidedness. A relation is found between the perimeter ratio and the number of polygons that would prove an interesting test for universal behavior in other networks. These laws are tested for invariance in changing gravity. This work adds bioconvection to the growing gallery of networks that abide by apparently universal constraints. Observed polygonal-side distributions are shown in Fig. 20 for bioconvection (present work), soap foams, Langmuir monolayers, and simulations.

The Stommel model for micro-organism circulation is applied to bioconvection. In qualitative agreement with the gravity dependence, the model also predicts the temperature and viscosity dependence of pattern-formation times. Future work will combine this picture of bioconvection to include the temperature dependence of active swimming and a more detailed analysis of the model’s gravity predictions.

- [1] D. Weaire and N. Rivier, *Contemp. Phys.* **25**, 59 (1984).
- [2] J. Stavans and J. A. Glazier, *Phys. Rev. Lett.* **62**, 1318 (1989).
- [3] J. A. Glazier, S. P. Gross, and J. Stavans, *Phys. Rev. A* **36**, 306 (1987).
- [4] C. Knobler, *Science* **249**, 870 (1990), and references cited therein.
- [5] H. Wager, *Philos. Trans. R. Soc. London, Ser. B* **201**, 333 (1911).
- [6] J. R. Platt, *Science* **133**, 1761 (1961).
- [7] H. Winet and T. L. Jahn, *Biorheol.* **9**, 87 (1972); S. Childress, M. Levandowsky, and E. A. Spiegel, *J. Fluid Mech.* **63**, 591 (1975). M. S. Plesset, C. Whipple, and H. Winet, *J. Theor. Biol.* **331**, (1976).
- [8] A. Harashima, M. Watanabe, and I. Fujishiro, *Phys. Fluids* **31**, 764 (1988).
- [9] J. O. Kessler, *Nature* **313**, 218 (1985).
- [10] A. M. Roberts, *Nature* **228**, 375 (1970).
- [11] T. J. Pedley and J. O. Kessler, *J. Fluid Mech.* **212**, 155 (1990) suggested a microgravity test of algal bioconvective patterns.
- [12] N. A. Hill, T. J. Pedley, and J. O. Kessler, *J. Fluid Mech.* **208**, 509 (1989).
- [13] T. L. Jahn, M. Brown, and H. Winet, *Am. Zoologist* **1**, 454 (1961); T. L. Jahn and M. Brown, *ibid.* **1**, 454 (1961); S. M. Gittleson, Ph.D. thesis, University of California, Los Angeles, 1966. Vortex entrainment of polystyrene spheres was measured up to a distance of 45  $\mu\text{m}$  from the cell surface of the algae, *Polytomella*.
- [14] M. Denehy, *Biol. Reprod.* **13**, 17 (1975). Vortex entrainment of polystyrene spheres was measured up to a distance of 60  $\mu\text{m}$  or one body length in ram sperm. J. J. L. Higdon, *J. Fluid Mech.* **94**, 305 (1979). Although the attractive nature of swimming in flagella remains complex, vortices were calculated to a maximum distance of eight times the flagellar-beating amplitude.
- [15] E. M. Shvirst, V. I. Krinskii, and G. R. Ivanitskii, *Biofiz.* **29**, 649 (1984) [*Biophys.* **29**, 710 (1984)].
- [16] J. J. Wille and C. F. Ehret, *J. Protozool.* **15**, 789 (1968) proposed the periodic synthesis of a mildly tacky substance to explain the circadian rhythm of bioconvective patterns in free-swimming *Tetrahymena*. S. Gittleson and T. Jahn, *J. Protozool.* **11**, Suppl. 13 (1964). For the algal species, *Polytomella parva*; A. J. Reynolds, *J. Fluid Mech.* **23**, 241 (1965) noted a similar boundary effect for individual swimmers, wherein a shear pattern directs swimming away from a wall. K. Brinkmann, *Z. Pflanzenphysiol.* **59**, 364 (1968); **59**, 12 (1968) suggested that a chemosensory response may play a role in *Euglena* patterns. Levandowsky (Ref. [23]) has reported chemotactic pattern formation in *Tetrahymena* (strain W) and the marine dinoflagellate *Cryptothecodinium cohnii*.
- [17] D. Noever, H. Matsos, J. Johnson, and R. Cronise (unpublished).
- [18] *Polytomella* cultures were prepared according to Ref. [13]. *Tetrahymena* cultures were prepared according to Winet and Jahn, Ref. [7].
- [19] T. Roenneberg, G. N. Colfax, and J. Hastings, *J. Biol. Rhythms* **4**, 201 (1989).
- [20] B. Berge, A. J. Simon, and A. Libchaber, *Phys. Rev. A* **41**, 6893 (1990).
- [21] N. Rivier, *Philos. Mag. B* **52**, 795 (1985).
- [22] T. J. Pedley, N. A. Hill, and J. O. Kessler, *J. Fluid Mech.* **195**, 223 (1988).
- [23] D. L. Koch and E. Shaqfeh, *J. Fluid Mech.* **209**, 521 (1989).
- [24] J. O. Kessler, *J. Fluid Mech.* **173**, 191 (1986).
- [25] J. Crowley, *Phys. Fluids* **19**, 1296 (1976); W. C. Thacker and J. W. Lavell, *ibid.* **21**, 291 (1978).
- [26] S. M. Gittleson and T. L. Jahn, *Exp. Cell. Res.* **51**, 579 (1968).
- [27] H. Winet and T. L. Jahn, *J. Theor. Biol.* **46**, 449 (1974).
- [28] J. O. Kessler, *Contemp. Phys.* **26**, 147 (1985).
- [29] M. Levandowsky, W. S. Childress, E. A. Spiegel, and S. H. Hutner, *J. Protozool.* **22**, 296 (1975).
- [30] E. M. Purcell, *Am. J. Phys.* **45**, 3 (1977).
- [31] S. M. Gittleson and T. L. Jahn, *Am. Nat.* **102**, 413 (1968).
- [32] H. Stommel, *J. Mar. Res.* **8**, 24 (1949).
- [33] J. B. Loefer and R. B. Mefferd, Jr., *Am. Nat.* **86**, 325 (1952).
- [34] See, e.g., F. Rosenberger, *Fundamentals of Crystal Growth I* (Springer-Verlag, Berlin, 1979), p. 273.
- [35] D. J. Srolovitz, M. P. Anderson, P. S. Sahni, and G. S. Grest, *Phys. Rev. Lett.* **50**, 263 (1983).
- [36] C. W. Beenakker, *Phys. Rev. Lett.* **57**, 2454 (1986).
- [37] K. Kawasaki, T. Nagai, and K. Nakashima, *Philos. Mag. B* **48**, 245 (1983).